

# Cost-optimal design of reverse electrodialysis process for salinity gradient-based electricity in desalination plants

*Energy*

C. Tristán<sup>a,\*</sup>, M. Fallanza<sup>a</sup>, I. Ortiz<sup>a</sup>, R. Ibáñez<sup>a</sup>, I. E. Grossmann<sup>b</sup>

<sup>a</sup> Department of Chemical and Biomolecular Engineering, University of Cantabria,  
Av. Los Castros 46, 39005 Santander, Spain.

<sup>b</sup> Department of Chemical Engineering, Carnegie Mellon University, Pittsburgh, PA 15213, USA

\*Corresponding author: [tristan@unican.es](mailto:tristan@unican.es)

## Abstract

This work provides the cost-optimal design of a large-scale reverse electrodialysis (RED) system deployed in a medium-capacity desalination plant (Canary Islands, Spain) using mathematical programming. The optimization model defines the hydraulic topology and working conditions of the RED units that maximize the net present value (NPV) of the RED process. We examine how past and future trends in electricity and carbon prices, membranes price, desalination plant capacity, and the use of high-conductive membranes may affect the competitiveness and performance of the NPV-optimal design. We also compare the conventional series-parallel configuration, and the optimal solution for the GDP model with recycling and added reuse alternatives of the RED units' exhausted streams to size the benefits of optimization over conventional heuristics. In the context of soaring electricity prices and strong green financing support, and the use of high-performing, affordable membranes ( $\sim 10$  €/m<sup>2</sup>), RED could save 8% of desalination plant energy demand from the grid earning profits of up to 5 million euros and LCOE of 66–126 €/MWh comparable to other renewable and conventional power technologies. In such conditions, the GDP model returns profitable designs for the entire range of medium-capacity desalination plants.

- 28 **Keywords:** Renewable energy; Generalized Disjunctive Programming; Desalination;
- 29 Wastewater reuse; Water-energy nexus.

## 30 **1 Introduction**

31 The energy released by mixing two water streams of different salinities, so-called salinity  
32 gradient energy (SGE), is a vast yet largely untapped renewable power source [1,2] to  
33 complement and diversify our current carbon and water-intensive energy mix [3–5], and  
34 sustain our energy-intensive water sector [6]. SGE technologies offer an integrated  
35 approach to the United Nations’ Sustainable Development Goal (SDG) 7 on affordable,  
36 reliable, sustainable energy access, and SDG 6 on clean water and sanitation.

37 Desalination and wastewater reuse are projected to increase in the coming decades [7,8]  
38 to reduce withdrawals from conventional surface and groundwater resources while  
39 meeting stringent water quality standards. However, as large energy users of conventional  
40 power sources [9,10], they are also large greenhouse gas (GHG) emitters that question  
41 their sustainability [11–13]. Seawater reverse osmosis (SWRO), the technology of choice  
42 in the global desalination market [14,15], is getting closer to the practical minimum  
43 energy to desalinate seawater hitting a record, low specific energy consumption (SEC) of  
44  $\sim 2$  kWh/m<sup>3</sup> of desalted water [9]. Despite the marked decline in SEC, the carbon footprint  
45 of large-scale desalination plants remains an issue [16,17]. Hence, coupling desalination  
46 with renewable energy sources will be vital for the sustainable production of desalinated  
47 water [13,18,19]. SGE technologies can provide clean, base-load electricity to  
48 desalination and wastewater treatment plants, supporting their decarbonization and  
49 circularity [6].

50 Within the SGE technologies, reverse electrodialysis (RED) has made great progress in  
51 the past two decades, and is now closer to commercialization with some pilot trials and  
52 field demonstrations [20–26]. In principle, a RED system takes in low- and high-salinity  
53 waters (LC and HC) on either side of alternate pairs of cation-exchange (CEM) and anion-  
54 exchange (AEM) membranes that let through counter-ions, but not co-ions and water

55 [27]. The salinity difference over each ion-exchange membrane (IEM) creates an  
56 electrochemical potential that drives the diffusion of cations through CEMs towards the  
57 cathode, and anions through AEMs towards the anode from the saltier stream to the less-  
58 salty side; redox reactions at the outer electrodes convert this ionic flow into an electron  
59 flux. The electric potential of the membrane pile and the resulting electric current can  
60 then be used to power the external load.

61 The low power density of large-scale RED (0.38–2.7 W/m<sup>2</sup> total membrane area), fouling,  
62 and high cost of commercial membranes are the main setbacks for RED technological  
63 readiness [1,28,29]. Niche markets beyond utility-scale electricity open new avenues to  
64 prove and advance RED market readiness. For instance, seawater desalination brine and  
65 wastewater are discarded streams that can be exploited to produce and save energy while  
66 minimizing the environmental impact of brine disposal [30]. Besides, desalination's  
67 seawater influent is already pre-treated to remove foulants [31], so the rejected brine  
68 would likely be less prone to cause fouling than raw seawater, which would require  
69 further energy-intensive purification.

70 While several studies have investigated the design of the RED process to improve the  
71 power density and/or the energy conversion efficiency (i.e., the fraction of SGE converted  
72 into useful work) of RED units in series or simple layouts, few have considered more  
73 complex topologies—which may yield optimal designs—and cost metrics (e.g., net  
74 present value, levelized cost of electricity), which are key drivers for widespread RED  
75 adoption [32–35]. Efficiency and power density are mutually exclusive performance  
76 metrics as maximizing both requires differing operating conditions [36]. Multi-staging of  
77 the RED stacks and electrode segmentation can provide efficient designs with higher  
78 power densities than once-through RED operation with unsegmented electrodes [37].  
79 Multi-staging adds to the design and operation space more degrees of freedom, such as

80 individual electrical control of the stages [38–40] like electrode segmentation [41–44],  
81 asymmetric staging (i.e., different spacer thickness, number of cell pairs, membrane  
82 properties, path length and type of mixing promoters in each stage) [37,45,46], and  
83 different configurations [40,44,47,48]. However, these studies do not consider the cost,  
84 which is a key enabler of RED technology adoption.

85 An alternative to making decisions about RED process design is to use optimization-  
86 based methods that rigorously search for the optimal configuration in a given design space  
87 [49]. Notably, Generalized Disjunctive Programming (GDP) [26] is a higher-level  
88 modeling framework that makes the formulation process more intuitive and systematic  
89 while preserving the underlying logic structure of the problem in the model [50]. Tristán  
90 et al. [51] developed a GDP optimization model that incorporates a detailed model of the  
91 RED stack [52,53] to define the hydraulic topology and the working conditions of a set  
92 of RED units that maximize the net present value (NPV) of the RED process. Their work  
93 illustrates the functionality and benefits of mathematical programming and GDP  
94 modeling on the conceptual design and optimization of the RED process over  
95 conventional heuristics.

96 This follow-up study applies the GDP optimization model [51] to define the cost-optimal  
97 design of a large-scale RED system in a medium-capacity SWRO desalination plant, a  
98 propitious market to prove and advance RED-based electricity. The assessment explores  
99 how electricity and emissions allowances prices over time, membranes price, SWRO  
100 desalination plant capacity, and membranes resistance, may affect the cost-optimal  
101 design, economic feasibility, and competitiveness of the RED process. To evaluate the  
102 benefits of the GDP model over heuristics, we also compare the conventional series-  
103 parallel configuration with the optimal solution to the GDP problem, which includes  
104 recycling and reuse alternatives of the exhausted streams of the RED units. This case

105 study serves to gauge the emissions and energy savings from the water- and carbon -  
106 intensive grid mix the RED system can offer to desalination in the most cost-conscious  
107 way, the way forward to make RED-based electricity a full-scale reality.

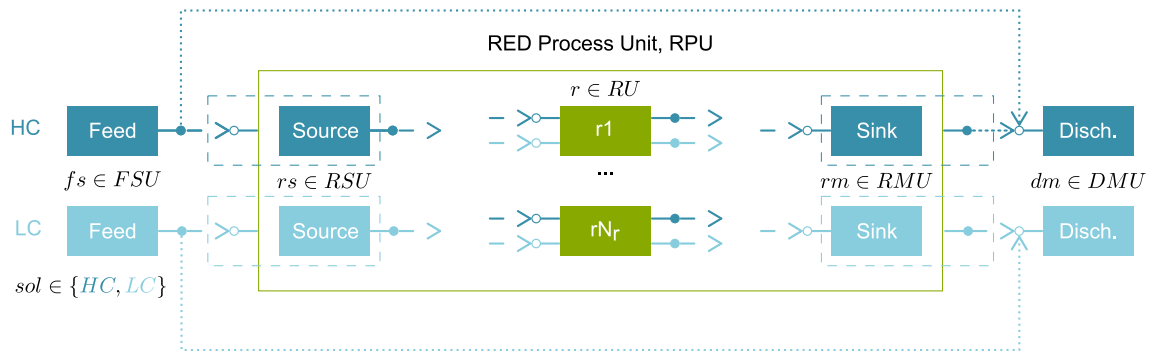
## 108 **2 Methods**

109 Optimization-based strategies involve three major steps: (i) postulating a superstructure  
110 that embeds the relevant flowsheet alternatives from which the optimum solution is  
111 selected, (ii) its formulation as a tractable mathematical programming model; and (iii)  
112 solving the model with an optimization algorithm to determine the optimal configuration  
113 [49,54]. Since the GDP model for the optimal design of the RED process is thoroughly  
114 described in [51], we will brief the reader on the main equations and assumptions.

### 115 **2.1 Problem statement and superstructure definition**

116 The problem addressed is to define the hydraulic topology, that is, the number and  
117 hydraulic arrangement of the RED units and their working conditions (e.g., electric  
118 current, inlet flow velocities, and molar concentrations) that yield the cost-optimal  
119 flowsheet design of the RED process for a given concentration, volume, and temperature  
120 of the high-salinity and low-salinity feed streams, and a fixed design of the RED stacks.

121 The superstructure in [Fig. 1](#) displays the feasible design alternatives for the stated  
122 problem, i.e., RED-based electricity production from the embedded energy of the HC and  
123 LC feed waste streams, with  $N_r$  conditional RED units. The reader is referred to [51] for  
124 details on the superstructure definition and notation.



125

126 **Fig. 1.** Superstructure for the RED process. High (HC) and low-salinity (LC) feed ( $fs \in$   
 127  $FSU$ ) and discharge ( $dm \in DMU$ ) units. The set of source ( $rs \in RSU$ ) and sink ( $rm \in$   
 128  $RMU$ ) units and the set of candidate RED units ( $r \in RU$ ) are children of the parent RED  
 129 Process unit ( $RPU$ ).

130 **2.2 Optimization model**

131 The set of equations (1) describes the general form of the non-convex Generalized  
 132 Disjunctive Programming (GDP) optimization model for the superstructure in [Fig. 1](#).  
 133 GDP models involve continuous and Boolean variables with constraints in the form of  
 134 algebraic expressions, conditional constraints within disjunctions, and logical  
 135 propositions. The  $Nr$  two-term disjunctions represent the discrete activation and  
 136 deactivation of the  $Nr$  candidate RED units.

$$\begin{aligned}
 \max NPV &= f(x) \\
 \text{s. t. } &g(x) \leq 0 \\
 &\left[ \begin{array}{c} Y_r \\ h_r(x) \leq 0 \end{array} \right] \vee \left[ \begin{array}{c} \neg Y_r \\ B^r x = 0 \end{array} \right] \quad \forall r \in RU \\
 &\Omega(Y_r) = True \\
 &x \in X \subseteq R^n \\
 &Y_r = \{True, False\} \quad \forall r \in RU
 \end{aligned} \tag{1}$$

138 In problem (1), the objective is to maximize the Net Present Value (NPV) of the RED  
 139 process subject to inequality constraints from process specifications and equality  
 140 constraints from material, energy balances, and thermodynamic relationships. The  
 141 continuous variables  $x$  are the molar concentrations and volumetric flows of the streams,  
 142 and the internal variables of the active RED units. Decisions are made on the electric  
 143 current and the concentration and flowrate of the RED stack's inlet streams. The global  
 144 constraints,  $g(x) \leq 0$ , outside the disjunctions are equalities and inequalities describing  
 145 specifications and physical relationships that apply for all feasible configurations in the  
 146 superstructure, e.g., mass balances of the feed, source, sink, and discharge units, and the  
 147 upper and lower bounds on concentration and flowrate. In each term of the disjunctions,  
 148 the Boolean variables  $Y_r$  govern the existence or absence of the RED unit; if a unit exists  
 149 or is selected ( $Y_r = True$ ), the associated active constraints  $h_r(x) \leq 0$  impose the  
 150 relevant mass and energy balances or other physicochemical phenomena that apply in the

151 RED unit, add the incurred capital and operating cost to the objective function, and set  
152 lower and upper bounds on its internal variables and the concentration and flowrate of its  
153 inlet and outlet streams; otherwise, the negation ( $\neg Y_r$ ) ignores the RED unit equations in  
154 the inactive disjunctive term, and  $B^r x = 0$  constraints set to zero a subset of the  
155 continuous variables and cost terms in the objective function. Other types of logical  
156 relationships for selecting the candidate RED units ( $\Omega(Y_r) = True$ ) are specified using  
157 logic propositions.

158 To formulate the GDP problem, we assume:

- 159 (a) The feed streams are pure sodium chloride (NaCl) solutions, thus neglecting the non-  
160 idealities of aqueous solution (i.e., unity activity coefficients) and the existence of  
161 other species that would undermine the RED performance.
- 162 (b) The internal losses depend only on the ionic resistance of solutions and membranes.
- 163 (c) Constant membranes permselectivity and ionic resistance apply, regardless of the  
164 solutions concentration and temperature.
- 165 (d) There is no water transport across the membranes against the concentration gradient  
166 due to osmosis, which implies a constant streamwise volumetric flowrate in RED's  
167 channel.
- 168 (e) Salt diffusivities in the membrane phase are independent of solutions concentration  
169 and temperature.
- 170 (f) No fluid leakage or ionic shortcut currents in the RED stack's manifolds.
- 171 (g) Co-current flow of the high- and low-concentration streams.
- 172 (h) The RED system operates under isothermal and isobaric conditions.

173 The solution to the GDP model maximizes the NPV of the RED process (2), which  
174 considers operating (OPEX in €/year), and capital costs (CAPEX in €) annualized over

175 the expected lifetime of the plant  $LT$  in years, using the capital recovery factor,  $CRF$ ,  
 176 given in (4) with a discount rate  $DR$ . The OPEX and annualized CAPEX define the total  
 177 annual cost (3),  $TAC$ , of the RED system. The NPV accounts for electricity sales and  
 178 carbon pricing revenues. The RED plant electricity is sold to the grid at Spanish average  
 179 price of electricity for non-house consumers,  $ep$  [55], and the abated GHG emissions  
 180 from the grid mix (Spanish emission factor,  $ef$ ) are subsidized at the average price,  $cp$ ,  
 181 in the European Union Emission Trading System (EU ETS) [56–60].

$$182 \quad NPV = \frac{(ep + cp ef) TNP LF - TAC}{CRF} \quad (2)$$

$$183 \quad TAC = CRF CAPEX + OPEX \quad (3)$$

$$184 \quad CRF = \frac{DR}{1 - (1 + DR)^{-LT}} \quad (4)$$

$$185 \quad TNP = \sum_{r \in RU} NP_r \quad (5)$$

186 We use a semi-rigorous version of Tristán et al. [51,52] RED stack model, to balance  
 187 model fidelity and tractability. When the RED unit is active ( $Y_r = \text{True}$ ), the discretized  
 188 model predicts the net power output,  $NP_r$ , that is added to the net power capacity of the  
 189 RED system, i.e., total net power,  $TNP$  in kW (5). When the RED unit is absent ( $\neg Y_r$ ) the  
 190 net power output is set to zero.

191 We consider plant downtime due to membrane cleaning and system maintenance by  
 192 applying a load factor,  $LF$ , to the annual energy yield (kWh/year) of the RED plant  
 193 working at full capacity.

194 To estimate the capital investment, we determine the cost of RED stacks,  $\sum_{r \in RU} CC_{stack,r}$ ,  
 195 pumps,  $CC_{pump}$ , and civil and electrical infrastructure costs,  $CC_{civil}$ .

196 
$$CAPEX = \sum_{r \in RU} CC_{stack,r} + CC_{pump} + CC_{civil} \quad (6)$$

197 The annual operating cost comprises the electricity cost from pumps,  $\sum_{r \in RU} OC_{pump,r}$ ,  
 198 the replacement cost of membranes,  $\sum_{r \in RU} OC_{IEMSrep,r}$ , and maintenance and labor costs.

199 
$$OPEX = \sum_{r \in RU} OC_{pump,r} + \sum_{r \in RU} OC_{IEMSrep,r} + 0.02 CAPEX \quad (7)$$

200 When the RED unit is active,  $CC_{stack,r}$  is added to CAPEX, and  $OC_{pump,r}$  and  $OC_{IEMSrep}$   
 201 to OPEX; otherwise, these terms take zero values.

202 The remainder financial parameters are those reported in Table 1.

203 **Table 1.** Financial parameters for the RED plant.

Parameter	Value
Plant lifetime, $LT$ (years)	30
Membranes' lifetime, $LT_m$ (years)	10
Load Factor, $LF$	90%
Discount rate, $DR$	5%
Spanish emission factor, $ef$ (kg CO <sub>2</sub> -eq/kWh)	0.374

204

### 205 **2.3 Solution strategy**

206 We code the GDP model using the Python-based, algebraic modeling language Pyomo  
 207 [61] and Pyomo.GDP, a Pyomo library extension for logic-based modeling and  
 208 optimization [62]. To solve the GDP problem, we apply the Global Logic-based Outer  
 209 Approximation (GLOA) algorithm [63,64] implemented in the logic-based solver  
 210 GDPopt version 20.2.28 built on Pyomo.GDP. The GLOA algorithm decomposes the  
 211 solution to the GDP into a sequence of mixed-integer linear programming (MILP) master  
 212 problems and reduced nonlinear programming (NLP) subproblems.

213 We solve the MILP master problems with CPLEX and the NLP subproblems with the  
 214 multistart heuristic algorithm MSNLP using IPOPTH as a local NLP solver on a machine

215 running Windows 10 (x64) with 6 cores processor (Intel® Core™ i7-8700 CPU @3.2  
 216 GHz) and 16 GB of RAM. We access the MINLP and NLP solvers from GAMS 34.1.0  
 217 through the Pyomo-GAMS interface. The stopping criteria depend upon the MSNLP  
 218 solver's maximum number of iterations (i.e., 500 NLP solver calls) to guarantee a near-  
 219 optimal solution.

## 220 **2.4 Techno-economic performance metrics**

221 To assess the technical performance of the optimal RED process designs, we determine  
 222 its net power density, i.e., the net power produced per membrane area, and its net energy  
 223 efficiency, or the fraction of exergy or theoretical maximum energy attainable in form of  
 224 SG, converted to useful work. We consider the Levelized Cost of Energy (LCOE) to  
 225 assess the cost-competitiveness of the RED optimal designs.

### 226 **Net and thermodynamic energy efficiency**

227 The exergy or Gibbs free energy of mixing is the theoretical maximum energy that is  
 228 available for useful work from a system reaching equilibrium. The difference in the Gibbs  
 229 free energy between the final mixture and the initial high and low-salinity solutions yields  
 230 the change in free energy of mixing of the inlet  $\Delta G_{mix,in}$  and outlet  $\Delta G_{mix,out}$  (8) streams  
 231 of the RED process unit, i.e. streams  $(fso, rsu)$  and  $(rmu, dmi)$  [41,65].

$$232 \quad \Delta G_{mix,i} = 2 R T \sum_{sol \in \{HC, LC\}} Q_{i,sol} C_{i,sol} \ln \frac{C_{i,sol}}{C_{M,i}} \quad (8)$$

$$\forall i \in in \cup out = (fso, rsu) \cup (rmu, dmi)$$

$$233 \quad C_{M,i} = \frac{\sum_{sol \in \{HC, LC\}} Q_{i,sol} C_{i,sol}}{\sum_{sol \in \{HC, LC\}} Q_{i,sol}} \quad (9)$$

$$\forall i \in in \cup out = (fso, rsu) \cup (rmu, dmi)$$

234 where  $R$  is the gas constant (8.314 J/mol/K),  $T$  is the absolute temperature (K), 2 denotes  
 235 the number of ions each NaCl molecule dissociates into,  $Q$  is the volumetric flowrate

236 ( $\text{m}^3/\text{s}$ ) and  $C$  the concentration ( $\text{mol}/\text{m}^3$ ) of the initial high and low-salinity solutions  
 237 entering and leaving the RED process. Equation (9) yields the concentration of the mixed  
 238 solution in thermodynamic equilibrium ( $C_M$  in  $\text{mol}/\text{m}^3$ ) of the RED process inflow and  
 239 outflow streams.

240 The net energy efficiency,  $\eta_{net}$ , measures the input fraction of free energy that RED  
 241 converts into electricity (10). The exergy change between RED process inlet and outlet  
 242 streams is the exergy recovered for conversion, i.e., the retrieved exergy for useful work  
 243 ( $\Delta G_{mix,retrieved}$ ), that is used to compute the thermodynamic efficiency,  $\eta_{th}$ , of the RED  
 244 process.

$$245 \quad \eta_{net} = \frac{TNP}{\Delta G_{mix,in}} \quad (10)$$

$$246 \quad \eta_{th} = \frac{TNP}{\Delta G_{mix,in} - \Delta G_{mix,out}} = \frac{TNP}{\Delta G_{mix,retrieved}} \quad (11)$$

## 247 **Levelized Cost of Energy (LCOE)**

248 The LCOE ( $\text{€}/\text{kWh}$ ) estimates the average cost per unit of energy generated across the  
 249 lifetime of a power plant that would break even the RED project costs. The LCOE gives  
 250 a first-order assessment of the RED project viability. Assuming the energy provided  
 251 annually is constant during the lifetime of the project, the LCOE reduces to (12).

$$252 \quad LCOE = \frac{CRF CAPEX + OPEX}{TNP 8760 LF} - cp ef \quad (12)$$

## 253 **2.5 Specifications for the RED optimal design deployed in a medium-size** 254 **desalination plant**

255 The large-scale RED system recovers energy from the concentrate effluent of  
 256 Maspalomas II SWRO desalination plant in Gran Canaria (Canary Islands, Spain) [66–  
 257 68]. Maspalomas II plant produces 26,184  $\text{m}^3/\text{day}$  of desalted water and rejects 17,602

258 m<sup>3</sup>/day of high-salinity brine (1.67 M NaCl, 20 °C) with a SEC of 3.77 kWh/m<sup>3</sup>. The low-  
 259 salinity feedwater (20mM NaCl) may be obtained from nearby wastewater treatment  
 260 plants (e.g., el Tablero, las Burras) [69]. Hence, we assume the same LC and HC feed  
 261 volume available for SGE conversion.

262 The case study explores how (i) electricity and carbon prices, (ii) membrane price, (iii)  
 263 desalination plant capacity, and (iv) membrane resistance, may affect the cost-  
 264 competitiveness, power density, and energy efficiency of the NPV-optimal RED design.  
 265 All the assessments refer to a commercial RED unit (Table 2) in 2022 unless otherwise  
 266 stated.

267 **Table 2.** Parameters of the commercial RED stack (Fumatech GmbH<sup>®</sup>, Germany).

<b>Parameter</b>	<b>Value</b>
Number of cell pairs	1000
Channel size	1.824 m × 1.532 m <sup>a</sup>
<b>Spacers</b>	
Thickness (μm)	270 <sup>b</sup>
Porosity	82.5%
<b>Membranes properties: fumasep<sup>®</sup> CEM (FKS-50) / AEM (FAS-50)</b>	
Areal resistance (Ω·cm <sup>2</sup> )	1.8 / 0.6 <sup>c</sup> (-20%) <sup>d</sup>
Permselectivity (-)	0.93
Thickness dry (μm)	50
Active area (m <sup>2</sup> )	0.7 <sup>a</sup>

268 <sup>a</sup> Four times the size of fumatech<sup>®</sup> ED-1750 pilot-scale module. <sup>b</sup> Equal to inter-  
 269 membrane distance i.e. HC or the LC channels height. <sup>c</sup> Measured in 0.5 M NaCl at 25  
 270 °C. <sup>d</sup> Reduction assuming future advances in membranes design.

271

272 To assess the influence of electricity price and carbon pricing over time, we gather  
 273 Spanish average electricity price [55] and EU ETS average emission allowances price  
 274 [70] for the period 2017–2022. We regress EU-27 data from 2007 onwards [55] to  
 275 estimate 2030 electricity prices; the carbon price in 2030 is a central estimate benchmark  
 276 from OECD [71]. We assess the sensitivity to membrane costs by setting (i) the current  
 277 price of membranes (i.e., average CEM and AEM cost from Fumatech<sup>®</sup>, 87.5 €/m<sup>2</sup>); and

278 (ii) the lowest price reported in the literature ( $\sim 10$  €/m<sup>2</sup>) [72]. We assume 20% drop in  
279 membranes resistance to reflect future advancements in membranes design. We reduce  
280 the flowrate of both HC and LC feedwaters to estimate the minimum SWRO desalination  
281 plant capacity that would allow the NPV-optimal RED process earn profits.

282 To evaluate the benefits of the GDP optimization model in RED process design over  
283 heuristic approaches, we compare two hydraulic arrangements each with the same  
284 number of candidate RED units (i.e.,  $N_r = 35$ ):

285 (i) Fixed series-parallel layout, from our previous assessment [52], where the RED  
286 system treats desalination concentrate into several identical parallel arrays of units in  
287 series, so neither recycling nor alternative reuse of the outlet streams is allowed. The  
288 objective is to maximize the total net power of the parallel branch, as it was set in our  
289 former study [52].

290 (ii) GDP layout, leaving the connection between the superstructure units free as a discrete  
291 decision. In this case, the objective is to maximize the NPV.

292 In the Series layout, we estimate the working conditions that maximize the net power of  
293 a stand-alone RED stack to fix the flowrate of the inlet streams to each parallel branch.  
294 We assume that the high and low salinity feedwaters are evenly split among the parallel  
295 branches, each with the same optimal configuration, so the net power output and costs of  
296 the RED system scale accordingly.

### 297 **3 Results and discussion**

298 For all the scenarios and the given parameters, each solution provides the NPV-optimal  
299 topology and decision variables that balance electricity production and capital and  
300 operating outlays increase. Discrete decisions include the working RED units and the

301 active water streams. Continuous decisions are the flowrate and concentration of the inlet  
302 streams and the electric current of each active RED stack.

303 It is worth noting that simplifications and assumptions of the RED stack model result in  
304 an overestimation of the net power output and, as such, an underestimation of the LCOE  
305 and an overestimation of the NPV.

### 306 **3.1 Electricity and carbon price assessment**

307 As expected, the upward trend of electricity and emissions allowances prices over time  
308 (Fig. 2) favors RED process techno-economic performance (Fig. 3), which in turn relieves  
309 the grid mix supply of Maspalomas II desalination plant (RED-based electricity could  
310 meet about ~7–8% of the SEC).

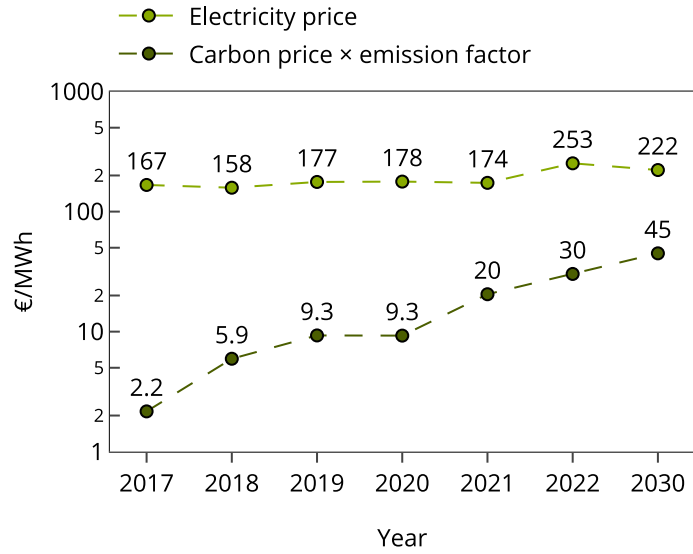
311 Russia's invasion of Ukraine in early 2022 brought severe disruptions in the EU energy  
312 market. The unprecedented surge in European fossil gas prices is echoed in the unparallel  
313 electricity price spike in 2022 (Fig. 2), soaring prices that incentives the promotion of  
314 emerging renewable technologies such as RED. Besides, the cap-and-trade EU ETS limits  
315 the volume of allowances in the market over time (Fig. 2) to comply with emissions  
316 reduction targets, the scarcity of emission allowances (among other factors) increases  
317 their price used in financing RED (Fig. 4).

318 For the assessed period (Fig. 4), electricity sales are the main revenue source, with lower  
319 yet growing revenue shares from auctioning allowances in the EU ETS (e.g., from 1% of  
320 all revenues in 2017 to ~11% in 2022 and ~17% in 2030). As a result, RED benefits grow  
321 by about 52% in five years, a 25% increase in NPV. Despite the slight decline of  
322 electricity price in 2030, the RED process may raise 724,155 euros each year during their  
323 lifetime yielding a NPV of about 4.4 million euros.

324 When electricity is priced high, the revenue gained outstrips the increase in costs from a  
325 larger number of RED units (Fig. 4). The optimal solution therefore activates more RED  
326 units to raise the nominal generation capacity of the RED system (10 units in five years  
327 delivering 23% more TNP), but at a cost. Each unit added to the RED system reduces the  
328 overall net power density from 2.1 W/m<sup>2</sup> in 2017 to 1.8 W/m<sup>2</sup> in 2022 (Fig. 3). On the  
329 flip side, the RED system retrieves more exergy for conversion (15% more exergy than  
330 in 2017) from which a greater share (39% in 2017 and 42% in 2022) is converted into net  
331 electricity, enhancing the overall energy efficiency and net power output of the RED  
332 system (Fig. 3).

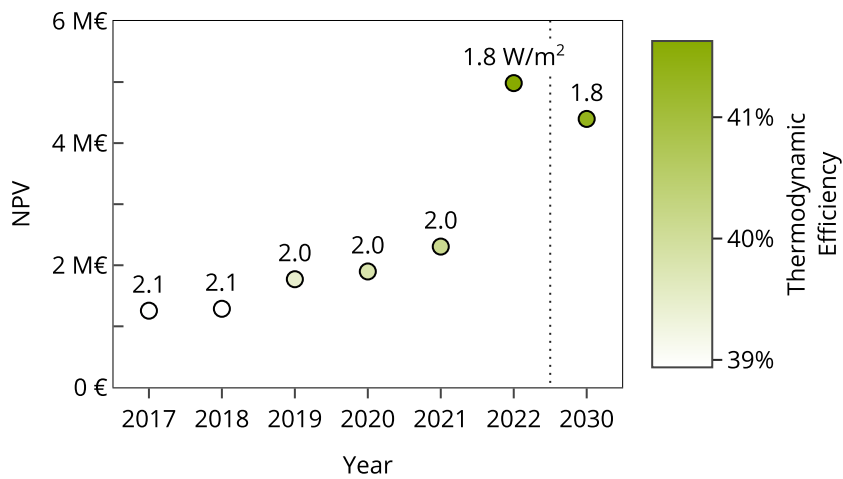
333 The overall net power density loss is related to the lower inlet flowrate of the RED units.  
334 This is because the same HC and LC feed volumes (kept constant throughout the years)  
335 are sourced to a larger number of RED units. Such lower inlet flowrate causes the RED  
336 units to depart from the net-power optimal working conditions, thereby reducing its  
337 power rate.

338 These findings indicate that in a context of high electricity prices and strong green  
339 financial support, RED technology does not require to reach the ambitious ~2.0 W/m<sup>2</sup> to  
340 be competitive as previous studies suggested. This is a reassuring result for RED  
341 transition from lab-scale to commercialization.



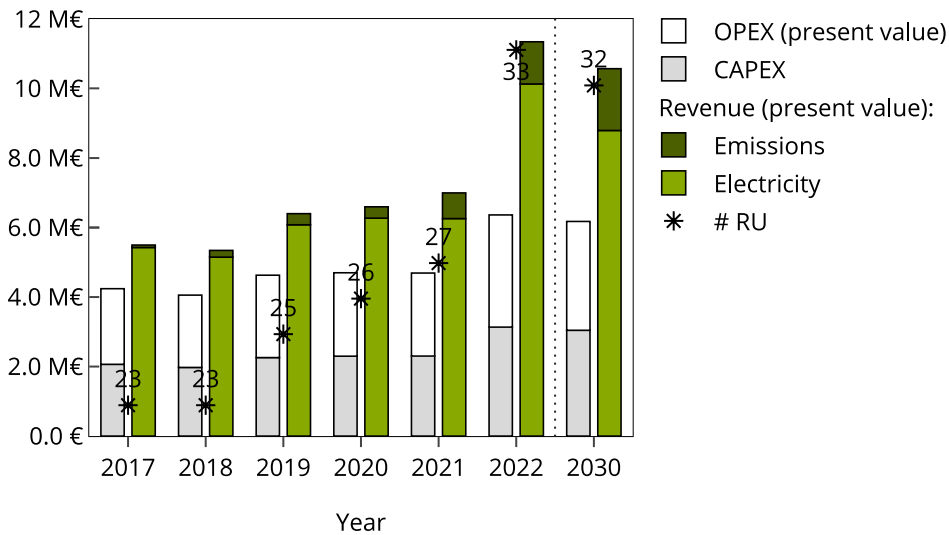
342

343 **Fig. 2.** Revenues per MWh from electricity and emission allowances over the period  
 344 2017–2022 with projections to 2030



345

346 **Fig. 3.** Net present value, net power density (markers text), and thermodynamic energy  
 347 efficiency (markers color) of the NPV-optimal RED process design over the past five  
 348 years from 2022 and forecast to 2030.



349

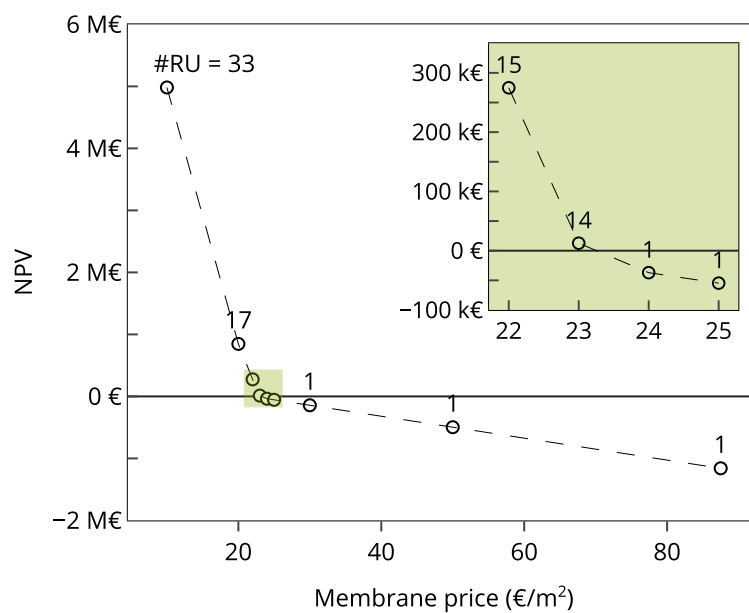
350 **Fig. 4.** NPV-optimal RED process over the period 2017–2022 with projections to 2030:  
 351 cost and revenues breakdown in present value and number of active RED units, # RU.

### 352 3.2 Membrane price assessment

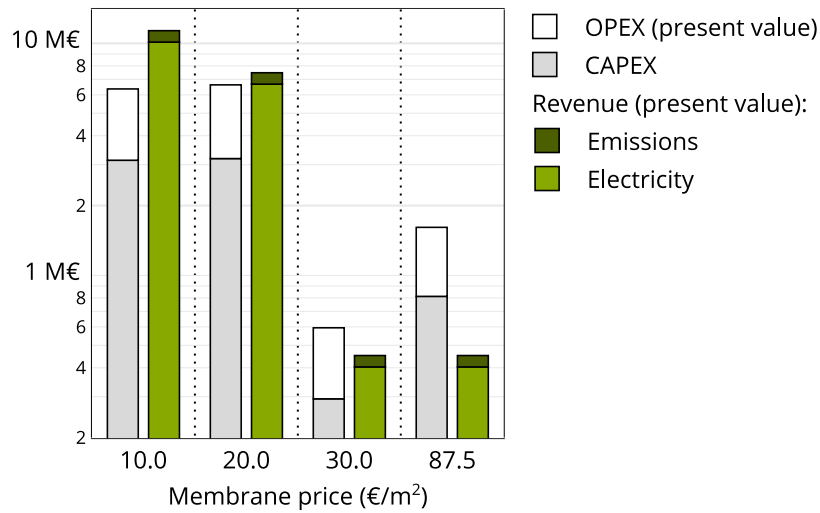
353 The membrane price that breaks even the NPV-optimal RED design falls somewhere  
 354 between 23 €/m<sup>2</sup> and 24 €/m<sup>2</sup> (Fig. 5Fig-5), just under twice to six times the price of  
 355 previous estimates of similar feeds concentrations (see Table 3Table-4). Membranes  
 356 priced above 23 €/m<sup>2</sup> yield larger economic losses when more than one RED unit is  
 357 active, that is, the capital and operational expenses overshadow incomes from electricity  
 358 sales and green financing incentives to a greater extent with an increasing number of  
 359 working RED units (Fig. 6Fig-6); therefore, the optimal RED process design keeps one  
 360 RED unit active under near-optimal working conditions (i.e., maximum net generation),  
 361 which results in a higher power density of 2.4 W/m<sup>2</sup> but reduced net (21%) and  
 362 thermodynamic (36%) efficiencies (Fig. 7Fig-7). As a result, the net power output and  
 363 the derived electricity and emissions revenues from a single RED unit remain unchanged,  
 364 whereas the investment and operational costs (i.e., membranes' replacement cost)  
 365 increase linearly with membrane price (Fig. 6Fig-6). The balance between the constant  
 366 revenues and higher total costs of a single but costlier RED stack is reflected in the linear  
 367 decline of NPV with membrane price (Fig. 5Fig-5).

368 The NPV trend shifts for membranes rated below 23 €/m<sup>2</sup>, following a steep increase with  
 369 lower membrane prices (Fig. 5). As membrane price falls the GDP model activates  
 370 more RED units since the revenues earned outweigh the increase in capital and operating  
 371 cost. The overall net power density decreases due to the larger number of RED units fed  
 372 with the same feed flowrate, which recover a larger fraction of the input exergy for  
 373 conversion increasing the net efficiency (Fig. 7). The thermodynamic efficiency  
 374 also increases because the active RED units operate at lower inlet flowrates, reducing the  
 375 overall pump power consumption.

376 With the abatement of membrane costs, designers can focus on achieving higher energy  
 377 recovery rates from SG, leading to the development of more efficient and economically  
 378 viable designs that increase the RED-based share of the SWRO desalination plant supply  
 379 from 0.3% from a single costlier RED unit to 8% from 33 cheaper RED units. The scale-  
 380 up of the RED process capacity to the MW order would likely make the project profitable  
 381 in the short run if cheaper manufacturing membrane processes lower its cost to ~20 €/m<sup>2</sup>.

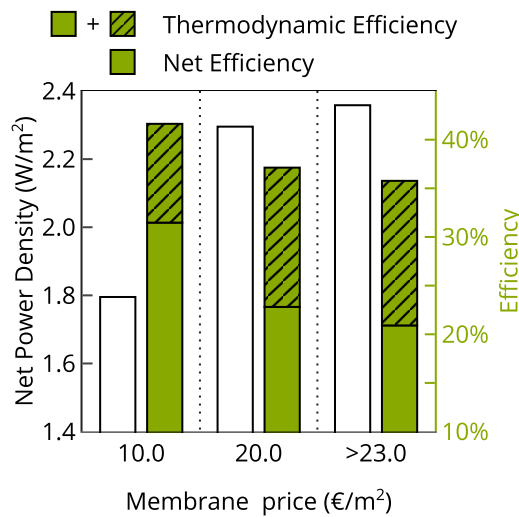


382  
 383 **Fig. 5.** Membrane price influence on the NPV-optimal RED process design: net present  
 384 value and number of active RED units. The inset magnifies the NPV in the membrane  
 385 price range within the boxed part of the graph.



386

387 **Fig. 6.** Membrane price influence on the NPV-optimal RED process design: cost and  
 388 revenues breakdown in present values.



389

390 **Fig. 7.** Membrane price influence on the NPV-optimal RED process design: net power  
 391 density, net and thermodynamic energy efficiencies.

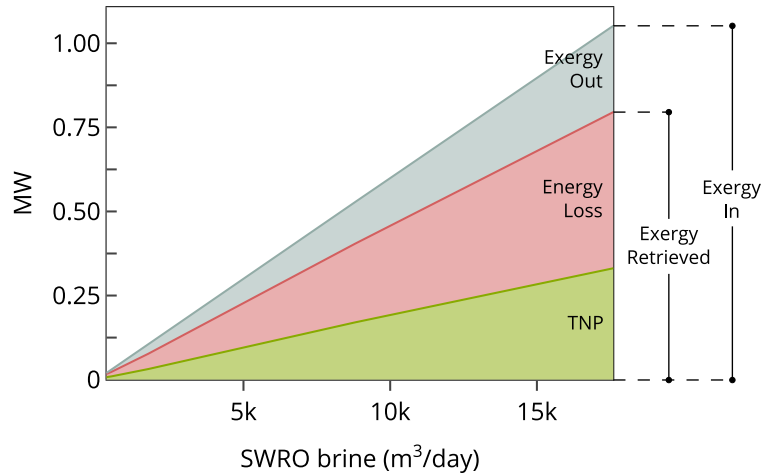
### 392 3.3 SWRO desalination plant capacity assessment

393 The available feeds flowrate restricts the exergy input which in turn bounds the useful  
 394 work of the RED process. The exergy input scales linearly with the desalination plant  
 395 capacity ([Fig. 8Fig-8](#)), and so does the TNP of the RED plant ([Fig. 8Fig-8](#) and markers  
 396 size in [Fig. 9Fig-9](#)). As such, to maximize the NPV with scarce feed volumes, the GDP  
 397 optimization model deactivates RED units (keeping a single RED unit in the low-end  
 398 capacity range of medium-sized SWRO desalination plants, i.e., 500 m<sup>3</sup>/day). By  
 399 reducing the number of RED units, the NPV-optimal RED process attempts to emulate

400 the overall working conditions with larger feed volumes. With larger HC and LC feed  
401 volumes (4400–17,600 m<sup>3</sup>/day) the NPV-optimal solution retrieves ~76% and converts  
402 ~31% of the input exergy into electricity (TNP) (Fig. 8). The net power density and  
403 thermodynamic efficiency remain roughly constant to ~1.8 W/m<sup>2</sup> and ~42% up to a tenth  
404 of Maspalomas II capacity. owing to the lower number of RED units (3 units) operating  
405 with larger, net-power optimal flowrates that increase the net power density to 1.9 W/m<sup>2</sup>  
406 with a slight decline in thermodynamic efficiency (41%).

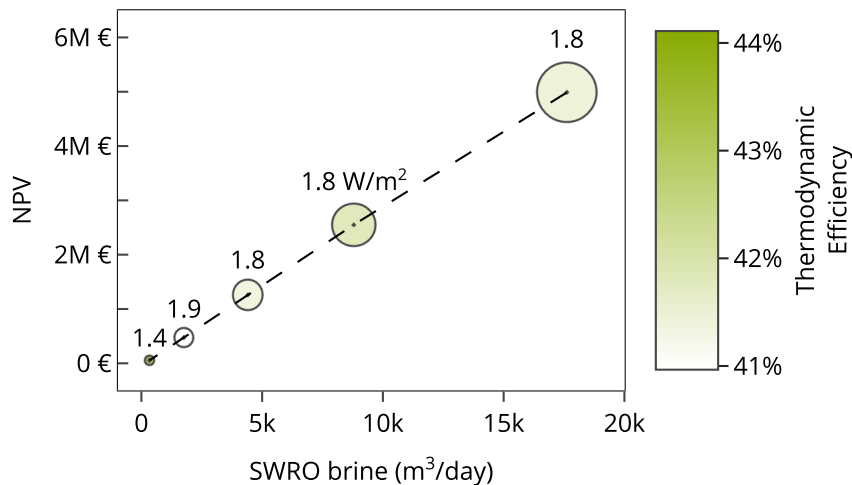
407 Desalination plants rejecting ~334 m<sup>3</sup>/day (i.e., 500 m<sup>3</sup>/day nominal capacity), would  
408 allow to install a single RED unit, that must run with a lower sub-optimal flowrate due to  
409 the scarce HC and LC feed flowrates, as such the net power density decreases to 1.4  
410 W/m<sup>2</sup>, while the energy efficiency increases to 44%. This is because the RED unit  
411 depletes to a greater extent the concentration gradient with lower hydrodynamic losses.  
412 Even so, the RED unit would source about 7.5 kW to the desalination plant reaping a  
413 profit of 53,595 euros.

414 Overall, the integration of on-site electricity generation based on RED technology in  
415 desalination plants of up to 500 m<sup>3</sup>/day capacity can alleviate the reliance on water and  
416 energy-intensive grid mixes, contributing to more sustainable and self-sufficient water  
417 supply systems.



418

419 **Fig. 8.** SWRO desalination plant capacity influence on the NPV-optimal RED process  
 420 design: energy balance.



421

422 **Fig. 9.** SWRO desalination plant capacity influence on the NPV-optimal RED process  
 423 design: net present value, net power density (markers text), total net power output  
 424 (markers size), and net thermodynamic efficiency (markers color).

425 **3.4 Membrane resistance assessment**

426 The use of high-performance membranes would provide slightly more powerful—i.e.,

427 7.4% more TNP with a 4.2% increase in the overall net power density (Fig. 10Figure

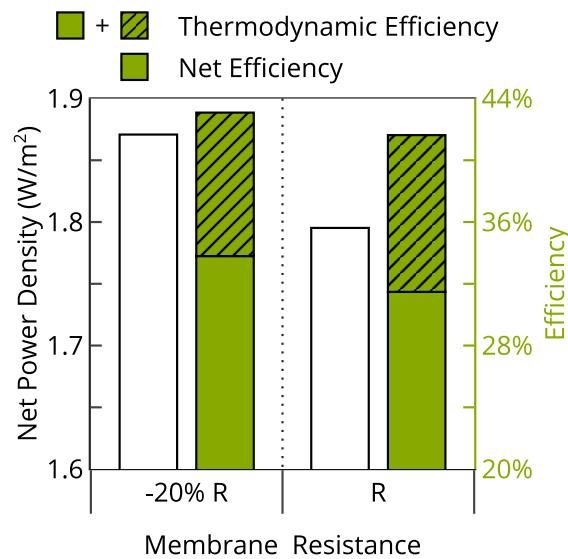
428 10)—and efficient designs—3.5% more efficient in terms of thermodynamic efficiency

429 (Fig. 10Figure-10)—by simply adding a RED unit to the RED system (about 5.6 km<sup>2</sup> of total

430 IEM area in a single stack). Such small improvement, however, would add up almost a

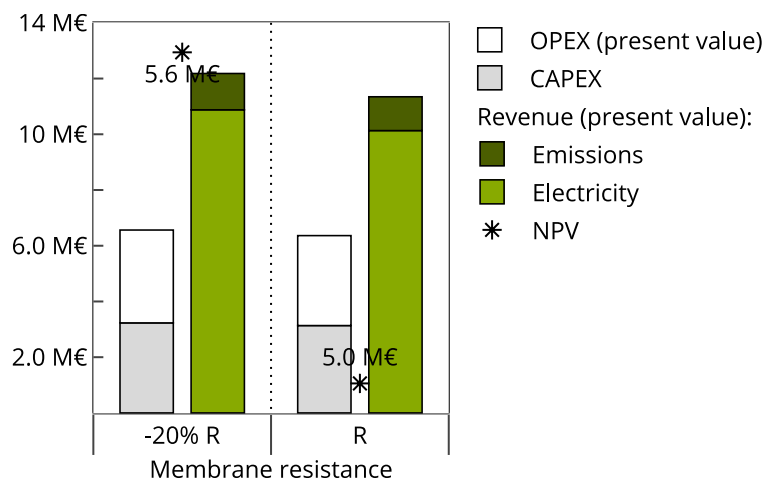
431 million euros of benefits with virtually no impact on capital and operational costs,

432 resulting in a 13% NPV growth (Fig. 11Fig. 11). The LCOE would also improve, moving  
 433 from 103 €/MWh to 97 €/MWh These results emphasize that any improvement in  
 434 membranes' performance has a positive impact on cost-competitiveness and widespread  
 435 adoption of RED, a solid reason to thrust the development of cost-effective manufacturing  
 436 processes and mass production of low-resistance membranes to reach prices of ~10 €/m<sup>2</sup>.



437

438 **Fig. 10.** Membrane resistance influence on the net power density, net and thermodynamic  
 439 energy efficiencies of the NPV-optimal design.



440

441 **Fig. 11.** Membrane resistance influence on the NPV-optimal design: cost and revenues  
 442 breakdown in present values and net present value (markers).

### 443 3.5 Conventional series-parallel layout vs. NPV-optimal layout

444 The optimal GDP layout outperforms the series-parallel arrangement, as it renders  
 445 economically viable RED process designs with almost equal energy and emissions

446 savings from the grid (~7% in the conventional layout and ~8% in the cost-optimal  
447 layout).

448 The optimal series-parallel design of the RED process that peaks the total net power  
449 output with (i) a fixed hydraulic arrangement of the RED units, (ii) fixed concentration  
450 and flowrate of the HC and LC inlet water streams, and (iii) leaving the number of  
451 working RED units and its electric current as single decision variables, is far from being  
452 profitable (negative NPV of 2.9 million euros, Fig. 12). The GDP optimization model  
453 activates the largest feasible number of RED units in series, i.e., 5 out of the 35 candidate  
454 RED units per parallel branch, to maximize the net power generation of the whole system.  
455 Even though the last RED units in the series increase the net power of the system, the  
456 RED unit's net power density well decreases from the first  $1.9 \text{ W/m}^2$  to the last  $\sim 7 \text{ mW/m}^2$   
457 which makes them prohibitively expensive.

458 While the net energy efficiency of the series layout (33%, Fig. 13) aligns with the  
459 estimated value to make RED technology competitive with other renewables (i.e., 40%)  
460 [22], the total net power density ( $0.9 \text{ W/m}^2$ , Fig. 13) falls well below the estimated value  
461 to make RED cost-competitive ( $2.0 \text{ W/m}^2$ ) [22]. The capital and operational expenses  
462 outweigh the benefits from electricity sales and green financing incentives which cover  
463 78% of the total costs, as seen in Fig. 12.

464 These results show that the optimal design from the technical perspective is not always  
465 the same from an economical viewpoint. The series configuration recovers a larger  
466 fraction of SGE at expense of lower power density that renders the RED process  
467 unprofitable.

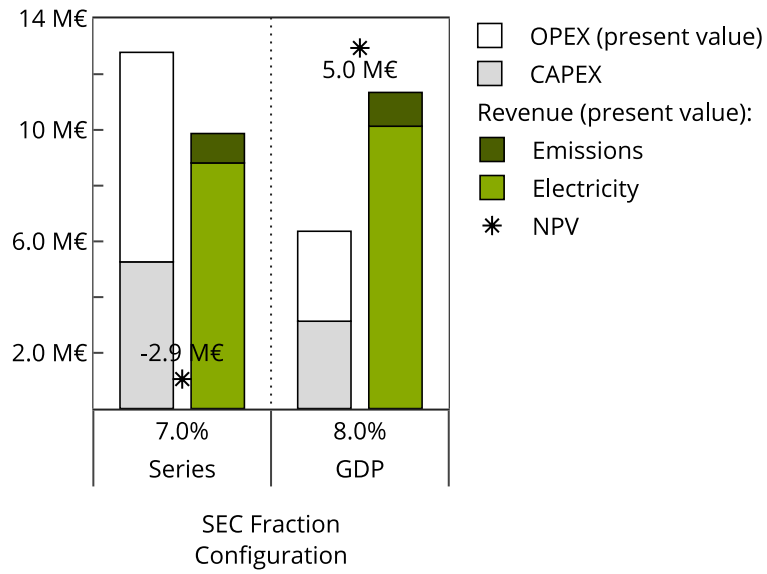
468 Even though the conventional layout retrieves more energy for conversion (by increasing  
469 the extent of mixing through the series), the input exergy is lower than the optimal GDP

470 layout (Fig. 14). This is because the total LC feed (assumed equal to Maspalomas II's  
471 desalination brine,  $\sim 733 \text{ m}^3/\text{h}$ ) restricts the number of parallel branches to 11. The optimal  
472 net-power inlet flowrate is about 0.6 times lower than the inlet LC flowrate, as such,  
473 around 42% of the brine remains untapped reducing the input exergy of the RED system  
474 to 866 kW.

475 As opposed to the series arrangement, the GDP layout, with its (i) larger volume of HC  
476 and LC feeds, and (ii) recycling and additional reuse alternatives, would provide cost-  
477 optimal designs that could earn hefty profits (Fig. 12) while reconciling high efficiency  
478 and higher power densities (Fig. 13). The reduced extent of mixing and lower pump  
479 consumption of the GDP layout (Fig. 14) improves the thermodynamic energy efficiency  
480 which increases from 35% in the series-parallel arrangement to 42% in the GDP layout  
481 (Fig. 13) despite the larger fraction of exergy unused (Fig. 14), which yields a modest  
482 decrease in net efficiency (Fig. 13).

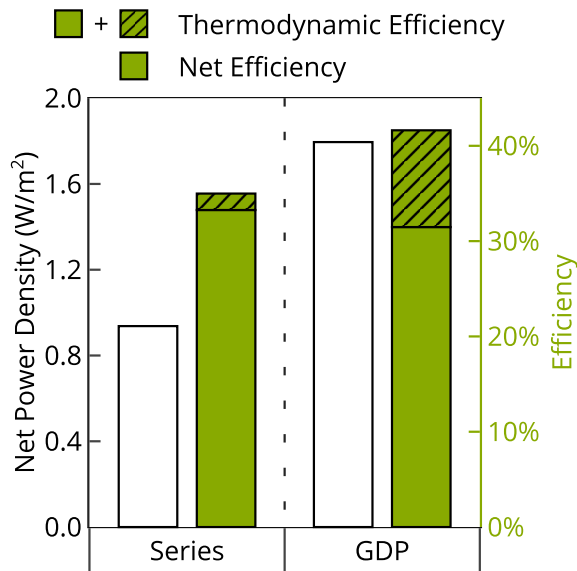
483 In the series-parallel arrangement, we enforce all RED units to work with higher flow  
484 velocities, those that peak the net power of the stand-alone RED unit (2.6 cm/s in the HC  
485 and 4.5 cm/s in the LC compartments). The effect of such high velocities is twofold: an  
486 overall pump power increase (eight times the GDP's), which in turn raises the investment  
487 and running costs (Fig. 12) and lowers the energy conversion efficiency (Loss in Fig. 14,  
488 and thermodynamic efficiency in Fig. 13).

489 These results underscore the value of mathematical programming and higher-level GDP  
490 modeling over heuristics for determining cost-optimal RED flowsheet designs.



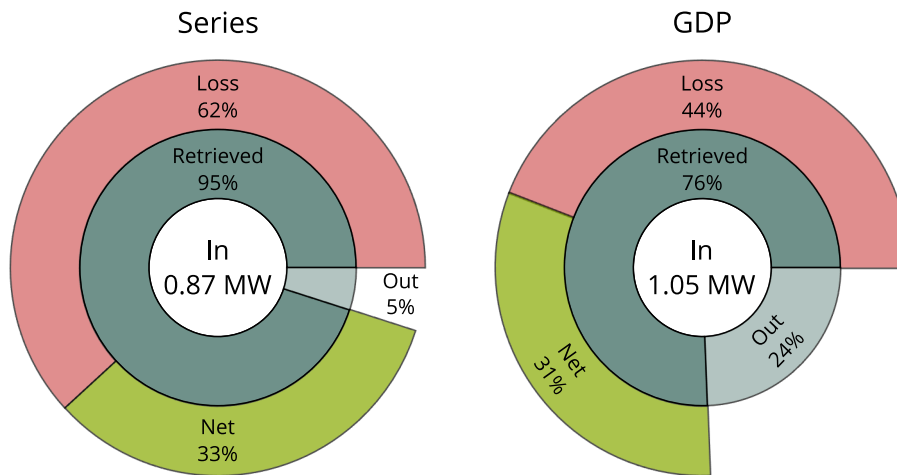
491

492 **Fig. 12.** Cost and revenues breakdown in present value and net present value of the series-  
 493 parallel and NPV-optimal layouts.



494

495 **Fig. 13.** Overall net power density, thermodynamic efficiency, and net energy efficiency  
 496 of the series-parallel and NPV-optimal layouts.



497

498 **Fig. 14.** Energy balance of the series-parallel and NPV-optimal layouts. In: Gibbs free  
 499 energy entering the RED system. Out: Gibbs free energy leaving the RED system unused.  
 500 Retrieved: Difference between input and output Gibbs free energies used for conversion  
 501 in the RED system. Loss: Gibbs free energy lost in energy conversion. Net: total net  
 502 power output of the RED system.

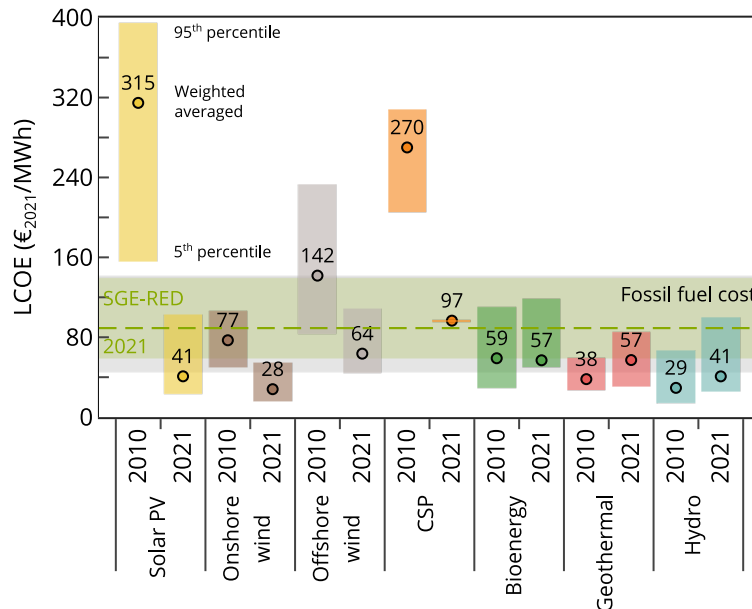
### 503 3.6 Contextualizing RED economic competitiveness

504 Despite the discrepancy between the assumptions and scale of renewables projects (i.e.,  
 505 utility-scale projects of at least 1 MW) in IRENA's LCOE estimates [73] and the NPV-  
 506 optimal LCOE of RED, [Fig. 15](#) provides some insights into RED competitiveness.

507 The assumed low membrane cost of 10 €/m<sup>2</sup> in all the assessed years would make the  
 508 LCOE of the NPV-optimal RED design fall within the range of fossil fuel-fired power  
 509 generation technologies ([Fig. 15](#)). In the face of soaring electricity prices and  
 510 stiffen emission reduction targets to be on track of 2030 Paris Agreement's goals, the  
 511 NPV-optimal RED process would even be on par (i.e., concentrated solar power, CSP) or  
 512 in the range of other renewables.

513 If similar trends of steep cost reduction, technological advancements, and high  
 514 penetration rates were to occur in RED technology, it is plausible that the LCOE for RED  
 515 could reach levels comparable to established renewable technologies such as solar  
 516 photovoltaic (PV) or onshore and offshore wind. This is in line with the steep cost  
 517 reductions witnessed in solar PV, CSP, and offshore wind over the past decade ([Fig.](#)

518 [15Fig. 15](#)). Even though IRENA’s analysis excludes the impact of government incentives  
 519 or subsidies, carbon emission pricing or the benefits of renewables in reducing other  
 520 externalities, these figures heighten the need in proving and advancing RED to reach  
 521 market-readiness.



522  
 523 **Fig. 15.** Global LCOE from newly commissioned, utility-scale renewable power  
 524 generation technologies, 2010-2020 [73]. NPV-optimal RED process LCOE range 2017–  
 525 2022 and 2030 (green filled area) and 2021 LCOE (green dashed line). Grey filled area  
 526 denotes price range of fossil fuel-fired technologies. All monetary values are in real, 2021  
 527 euros considering inflation and applying the exchange rate for each year. PV:  
 528 photovoltaic; CSP: concentrating solar power.

529 Table 5 compares reported cost estimates of RED and the LCOE of the NPV-optimal  
 530 RED process designs for current and future membrane price scenarios in 2022. The  
 531 paucity of detailed economic evaluations and wide variability in LCOE (16–4956  
 532 €/MWh) across existing studies due to disparity in their underlying financial and process  
 533 assumptions, makes any comparison inconclusive and open to discussion. As such, it  
 534 serves to extract some general guidelines and trends.

535 The HC and LC feed concentration, volume, and temperature determine the input exergy  
 536 and, thus, the nominal capacity and cost of the RED process. HC sources such as brines  
 537 from coal mines, desalination, saltworks, salt lakes, or regenerated thermolytic salt

538 solutions used in the so-called RED heat engines (1–5 M), offer higher SGE potential  
539 than less salty water bodies such as seawater (0.5–0.6 M). A purposely designed RED  
540 system could efficiently exploit these high-salinity sources, thus, reducing the LCOE.

541 Depending on the source, the feeds' pureness also may affect the performance and  
542 durability of RED if not properly pre-treated which may increase capital and operational  
543 expenses. In this work, the objective function, i.e., the NPV, exclude pre-treatment cost,  
544 which is likely to result in an underestimation of the actual LCOE for RED systems that  
545 use sources with extensive pre-treatment requirements, e.g., treated wastewater effluents,  
546 raw seawater, or river water.

547 None of the reported cost estimates in Table 5 consider the working conditions of each  
548 RED stack and their relative arrangement that may greatly improve both the performance  
549 and cost of the RED process as seen in the case study. Instead, most of them derived the  
550 cost of RED electricity or the LCOE for an estimated or projected RED unit power density  
551 or a targeted nominal capacity of the RED plant. Some also considered the impact of  
552 availability, concentration, and fouling potential of the HC and LC feeds, different RED  
553 stack sizes, and IEMs properties on RED system costs under fixed, suboptimal working  
554 conditions of the RED units. Such detailed assessments, however, miss cost-optimal  
555 design alternatives that optimization-based approaches can effectively handle and  
556 identify.

557 The case study and the reviewed studies reveal that realizing high-performing (i.e., low-  
558 resistant, high-permeable), affordable membranes is a crucial lever for RED techno-  
559 economic progress toward market competitiveness. As shown in the case study,  
560 membrane cost weighs heavily on the objective function. Even though all scenarios have  
561 equal feedstreams conditions and candidate RED units, the high price of commercial  
562 membranes makes the NPV-optimal design uneconomic. Only if IEMs were one-order-

563 of-magnitude cheaper, such that revenues offset the outlays increase, the NPV-optimal  
564 design would retain more RED units tuning their working conditions such that they reach  
565 the net power density that maximize the NPV. The cumulative experience in operating  
566 and developing RED technology will likely decline its LCOE to the estimated 66–126  
567 €/MWh.

**Table 34** Cost estimates of RED reported in the literature and the present study. TP: Total power. PD: Power density.

	High-salinity solution	Low-salinity solution	TP (MW)	PD (W/m <sup>2</sup> )	Capacity Factor	Lifetime [years]		IEMs Price (€/m <sup>2</sup> )	r	LCOE <sup>f</sup> (€/MWh)
						Plant	IEMs			
Turek (2007) [74]	0.6 M	9.6 mM	NR	0.46 <sup>a</sup>	NR	NR	10	68 (\$100/m <sup>2</sup> ) <sup>c</sup>	NR	4956 (6790) <sup>c</sup>
Turek (2008) [75]	1.9 M	9.6 mM	NR	1.04 <sup>a</sup>	NR	NR	10	68 (\$100/m <sup>2</sup> ) <sup>d</sup>	NR	2041 (3000) <sup>c</sup>
Post et al. (2010) [22]	0.5 M	5 mM	0.2	2 <sup>a</sup>	91%	20	7	2 10	6%	79 200
Daniilidis et al. (2014) [35]	0.5 M	17 mM	200	2.2 <sup>b</sup> 2.7 <sup>b</sup>	84%	25	7	4.3, 50 4	10%	18, 71 16
Weiner et al. (2015) [76]	0.6 M	17 mM	NR	1.2 <sup>b</sup>	NR	20	NR	676 (\$750/m <sup>2</sup> ) <sup>c</sup>	6%	5705 (6330)
Bevacqua et al. (2017) <sup>g</sup> [77]	2.6 M NH <sub>4</sub> HCO <sub>3</sub>	75 mM NH <sub>4</sub> HCO <sub>3</sub>	0.1 <sup>a</sup>	4.30	91%	20	NR	50	6%	683
	2.4 M NH <sub>4</sub> HCO <sub>3</sub>	10 mM NH <sub>4</sub> HCO <sub>3</sub>		2.39						
	2.5 M NH <sub>4</sub> HCO <sub>3</sub>	40 mM NH <sub>4</sub> HCO <sub>3</sub>		4.06						
Micari et al. (2019) <sup>g</sup> [78]	5 M	10 mM	1 <sup>b</sup>	3.2	90%	30	10	30	5%	400
Papapetrou et al. (2019) <sup>g</sup> [33]	3.8 M	10 mM	0.1	0.66 <sup>b</sup>	90%	30	10	30	5%	1360
	5 M	10 mM	1	4.67 <sup>b</sup>						
Giacalone et al. (2019) [34]	1.2 M	17 mM	2 <sup>b</sup> 4 <sup>b</sup>	1 <sup>a</sup> 2 <sup>a</sup>	90%	30	10	15 4, 15 15	5%	500 110, 250 270–330
	5 M	< 103 mM	0.01–1 <sup>b</sup> 0.04–3 <sup>b</sup>	1.5–2 <sup>a</sup> 6.5 <sup>a</sup>						
Ranade et al. (2022) [79]	5 M	0.5 M	0.015	1.19 <sup>b</sup>	82%	20	10	5, 50	5%	250, 1500
			0.031	2.44 <sup>b</sup>						
This work <sup>h</sup>	1.67 M	20 mM	0.327	1.8 <sup>b</sup>	90%	30	10	10 87.5	5%	98 998
			0.013	2.3 <sup>b</sup>						

<sup>a</sup> Gross power. <sup>b</sup> Net power. <sup>c</sup> Total investment cost. <sup>d</sup> Including endplates and electrodes. <sup>e</sup> Cost of electricity. <sup>f</sup> Values between brackets in \$/MWh converted to €/MWh with the corresponding year average exchange ratio from the International Monetary Fund (IMF). <sup>g</sup> RED heat engine. <sup>h</sup> Circa 2022.

#### 571 4 Conclusions

572 RED technology has great prospects in solving the water-energy challenge but needs to  
573 prove that it can generate electricity reliably to gain the trust of investors and  
574 manufacturers to unlock economies-of-scale cost reduction. In this work, we have  
575 presented an optimization model to devise techno-economic viable RED process designs  
576 that support the leap from lab to market. The Generalized Disjunctive Programming  
577 (GDP) model allowed us to define the hydraulic topology and working conditions of a set  
578 of RED units to maximize the net present value of the RED process deployed in a  
579 medium-capacity seawater reverse osmosis plant.

580 We have estimated the energy and emissions savings from the grid RED-based electricity  
581 may offer to desalination exploring relevant factors involved in the cost-optimal design  
582 of the RED process. The growing electricity and emission allowance prices over time  
583 strengthen RED market readiness in niche applications such as desalination and  
584 wastewater treatment sectors, reaching LCOE of 66–126 €/MWh on par or in the range  
585 of other renewable and conventional power technologies. A realistic near-term reduction  
586 in membrane price ( $\sim 20$  €/m<sup>2</sup>) would make RED profitable. The NPV-optimal RED  
587 process design may reap profits in medium-capacity SWRO desalination plants of up to  
588 500 m<sup>3</sup>/day. The use of low-resistance, low-cost membranes does improve the cost-  
589 competitiveness of the RED process; a 20% drop in membranes resistance would increase  
590 profits by 13%.

591 Expanding the operating decision space with recycling and reusing alternatives brings on  
592 RED process designs that not only attain profits while cutting down grid mix emissions,  
593 but also accommodate higher power densities and energy efficiencies. Indeed, with a  
594 slightly lower RED-based take of the total desalination energy demand ( $\sim 7\%$  in the series-  
595 parallel and  $\sim 8\%$  the NPV-optimal layouts), the series-parallel layout is as efficient as the

596 GDP layout at the expense of a significant drop in power density which bears large  
597 economic losses.

598 These assessments show mathematical programming is an efficient and systematic  
599 modeling and optimization tool to assist early-stage research, and to extract optimal  
600 design and operation guidelines for full-scale RED implementation.

601 **CReditTe authorship contribution statement**

602 **Carolina Tristán:** Conceptualization, Methodology, Software, Validation, Formal  
603 analysis, Investigation, Data curation, Writing - Original Draft, Visualization. **Marcos**  
604 **Fallanza:** Conceptualization, Writing - Review & Editing, Supervision. **Raquel Ibáñez:**  
605 Conceptualization, Resources, Writing - Review & Editing, Supervision, Project  
606 administration, Funding acquisition. **Inmaculada Ortiz:** Resources, Funding  
607 acquisition. **Ignacio E. Grossmann:** Conceptualization, Methodology, Resources,  
608 Writing - Review & Editing, Supervision

609 **Acknowledgments**

610 This work was supported by the LIFE Programme of the European Union (LIFE19  
611 ENV/ES/000143); the MCIN/AEI/10.13039/501100011033 and “European Union  
612 NextGenerationEU/PRTR” (PDC2021-120786-I00); and by the  
613 MCIN/AEI/10.13039/501100011033 and “ESF Investing in your future” (PRE2018-  
614 086454)

615 **References**

- 616 [1] Tufa RA, Pawlowski S, Veerman J, Bouzek K, Fontananova E, di Profio G, et al.  
617 Progress and prospects in reverse electro dialysis for salinity gradient energy  
618 conversion and storage. *Appl Energy* 2018;225:290–331.  
619 <https://doi.org/10.1016/J.APENERGY.2018.04.111>.
- 620 [2] Logan BE, Elimelech M. Membrane-based processes for sustainable power  
621 generation using water. *Nature* 2012;488:313–9.  
622 <https://doi.org/10.1038/nature11477>.
- 623 [3] Van Vliet MTH, Wiberg D, Leduc S, Riahi K. Power-generation system  
624 vulnerability and adaptation to changes in climate and water resources. *Nat Clim*  
625 *Chang* 2016;6:375–80. <https://doi.org/10.1038/nclimate2903>.
- 626 [4] Adamovic M, Bisselink B, De Felice M, De Roo A, Dorati C, Ganora D, et al.  
627 Water – Energy Nexus in Europe. Luxembourg: Publications Office of the  
628 European Union; 2019. <https://doi.org/10.2760/968197>.
- 629 [5] Behrens P, van Vliet MTH, Nanninga T, Walsh B, Rodrigues JFD. Climate change  
630 and the vulnerability of electricity generation to water stress in the European  
631 Union. *Nat Energy* 2017;2:1–7. <https://doi.org/10.1038/nenergy.2017.114>.

- 632 [6] Rani A, Snyder SW, Kim H, Lei Z, Pan SY. Pathways to a net-zero-carbon water  
633 sector through energy-extracting wastewater technologies. *Npj Clean Water* 2022  
634 51 2022;5:1–17. <https://doi.org/10.1038/s41545-022-00197-8>.
- 635 [7] IEA. WEO-2016 Special Report: Water-Energy Nexus. Paris: 2016.  
636 <https://doi.org/10.1021/es2016632>.
- 637 [8] van Vliet MTH, Jones ER, Flörke M, Franssen WHP, Hanasaki N, Wada Y, et al.  
638 Global water scarcity including surface water quality and expansions of clean  
639 water technologies. *Environ Res Lett* 2021;16:024020.  
640 <https://doi.org/10.1088/1748-9326/ABBFC3>.
- 641 [9] Voutchkov N. Energy use for membrane seawater desalination – current status and  
642 trends. *Desalination* 2018;431:2–14. <https://doi.org/10.1016/j.desal.2017.10.033>.
- 643 [10] Schunke AJ, Hernandez Herrera GA, Padhye L, Berry T-AA. Energy Recovery in  
644 SWRO Desalination: Current Status and New Possibilities. *Front Sustain Cities*  
645 2020;2:9. <https://doi.org/10.3389/FRSC.2020.00009>.
- 646 [11] Cornejo PK, Santana MVE, Hokanson DR, Mihelcic JR, Zhang Q. Carbon  
647 footprint of water reuse and desalination: a review of greenhouse gas emissions  
648 and estimation tools. *J Water Reuse Desalin* 2014;4:238–52.  
649 <https://doi.org/10.2166/WRD.2014.058>.
- 650 [12] Parkinson S. Guiding urban water management towards 1.5 °C. *Npj Clean Water*  
651 2021;4:1–6. <https://doi.org/10.1038/s41545-021-00126-1>.
- 652 [13] Alliance GCWD. Global Clean Water Desalination Alliance “H2O minus CO2.”  
653 2015.
- 654 [14] Eke J, Yusuf A, Giwa A, Sodiq A. The global status of desalination: An assessment  
655 of current desalination technologies, plants and capacity. *Desalination*  
656 2020;495:114633. <https://doi.org/10.1016/J.DESAL.2020.114633>.
- 657 [15] Jones E, Qadir M, van Vliet MTH, Smakhtin V, Kang S. The state of desalination  
658 and brine production: A global outlook. *Sci Total Environ* 2019;657:1343–56.  
659 <https://doi.org/10.1016/J.SCITOTENV.2018.12.076>.
- 660 [16] Pistocchi A, Bleninger T, Breyer C, Caldera U, Dorati C, Ganora D, et al. Can  
661 seawater desalination be a win-win fix to our water cycle? *Water Res*  
662 2020;182:115906. <https://doi.org/10.1016/J.WATRES.2020.115906>.
- 663 [17] Elimelech M, Phillip WA. The Future of Seawater Desalination: Energy,  
664 Technology, and the Environment. *Science* (80- ) 2011;333:712–7.  
665 <https://doi.org/10.1126/science.1200488>.
- 666 [18] Bundschuh J, Kaczmarczyk M, Ghaffour N, Tomaszewska B. State-of-the-art of  
667 renewable energy sources used in water desalination: Present and future prospects.  
668 *Desalination* 2021;508:115035. <https://doi.org/10.1016/J.DESAL.2021.115035>.
- 669 [19] Goh PS, Liang YY, Ismail AF. Energy Efficient Seawater Desalination: Strategies  
670 and Opportunities. *Energy Technol* 2021;9:2100008.  
671 <https://doi.org/10.1002/ENTE.202100008>.

- 672 [20] Nam J-Y, Hwang K-S, Kim H-C, Jeong H, Kim H, Jwa E, et al. Assessing the  
673 behavior of the feed-water constituents of a pilot-scale 1000-cell-pair reverse  
674 electro dialysis with seawater and municipal wastewater effluent. *Water Res*  
675 2019;148:261–71. <https://doi.org/10.1016/J.WATRES.2018.10.054>.
- 676 [21] Tedesco M, Cipollina A, Tamburini A, Micale G. Towards 1 kW power production  
677 in a reverse electro dialysis pilot plant with saline waters and concentrated brines.  
678 *J Memb Sci* 2017;522:226–36. <https://doi.org/10.1016/j.memsci.2016.09.015>.
- 679 [22] Post JW, Goeting CH, Valk J, Goinga S, Veerman J, Hamelers HVM, et al.  
680 Towards implementation of reverse electro dialysis for power generation from  
681 salinity gradients. *Desalin Water Treat* 2010;16:182–93.  
682 <https://doi.org/10.5004/dwt.2010.1093>.
- 683 [23] Kempener R, Neumann F. Salinity Gradient Energy Technology Brief. IRENA  
684 Ocean Energy Technol 2014.
- 685 [24] Jang J, Kang Y, Han JH, Jang K, Kim CM, Kim IS. Developments and future  
686 prospects of reverse electro dialysis for salinity gradient power generation:  
687 Influence of ion exchange membranes and electrodes. *Desalination*  
688 2020;491:114540. <https://doi.org/10.1016/j.desal.2020.114540>.
- 689 [25] IRENA. Innovation outlook: Ocean energy technologies. 2020.
- 690 [26] Mehdizadeh S, Kakihana Y, Abo T, Yuan Q, Higa M. Power generation  
691 performance of a pilot-scale reverse electro dialysis using monovalent selective  
692 ion-exchange membranes. *Membranes (Basel)* 2021;11:27.  
693 <https://doi.org/10.3390/MEMBRANES11010027>.
- 694 [27] Pattle RE. Production of Electric Power by mixing Fresh and Salt Water in the  
695 Hydroelectric Pile. *Nature* 1954;174:660–660. <https://doi.org/10.1038/174660a0>.
- 696 [28] Chae S, Kim H, Gi Hong J, Jang J, Higa M, Pishnamazi M, et al. Clean power  
697 generation from salinity gradient using reverse electro dialysis technologies:  
698 Recent advances, bottlenecks, and future direction. *Chem Eng J* 2023;452:139482.  
699 <https://doi.org/10.1016/J.CEJ.2022.139482>.
- 700 [29] Nazif A, Karkhanечи H, Saljoughi E, Mousavi SM, Matsuyama H. Recent  
701 progress in membrane development, affecting parameters, and applications of  
702 reverse electro dialysis: A review. *J Water Process Eng* 2022;47:102706.  
703 <https://doi.org/10.1016/J.JWPE.2022.102706>.
- 704 [30] Li W, Krantz WB, Cornelissen ER, Post JW, Verliefde ARD, Tang CY. A novel  
705 hybrid process of reverse electro dialysis and reverse osmosis for low energy  
706 seawater desalination and brine management. *Appl Energy* 2013;104:592–602.  
707 <https://doi.org/10.1016/j.apenergy.2012.11.064>.
- 708 [31] Badruzzaman M, Voutchkov N, Weinrich L, Jacangelo JG. Selection of  
709 pretreatment technologies for seawater reverse osmosis plants: A review.  
710 *Desalination* 2019;449:78–91. <https://doi.org/10.1016/j.desal.2018.10.006>.
- 711 [32] Weiner AM, McGovern RK, Lienhard V JH. Increasing the power density and  
712 reducing the levelized cost of electricity of a reverse electro dialysis stack through  
713 blending. *Desalination* 2015;369:140–8.

- 714 <https://doi.org/10.1016/j.desal.2015.04.031>.
- 715 [33] Papapetrou M, Kosmadakis G, Giacalone F, Ortega-Delgado B, Cipollina A,  
716 Tamburini A, et al. Evaluation of the Economic and Environmental Performance  
717 of Low-Temperature Heat to Power Conversion using a Reverse Electrodialysis –  
718 Multi-Effect Distillation System. *Energies* 2019;12:3206.  
719 <https://doi.org/10.3390/en12173206>.
- 720 [34] Giacalone F, Papapetrou M, Kosmadakis G, Tamburini A, Micale G, Cipollina A.  
721 Application of reverse electrodialysis to site-specific types of saline solutions: A  
722 techno-economic assessment. *Energy* 2019;181:532–47.  
723 <https://doi.org/10.1016/j.energy.2019.05.161>.
- 724 [35] Daniilidis A, Herber R, Vermaas DA. Upscale potential and financial feasibility of  
725 a reverse electrodialysis power plant. *Appl Energy* 2014;119:257–65.  
726 <https://doi.org/10.1016/j.apenergy.2013.12.066>.
- 727 [36] Yip NY, Brogioli D, Hamelers HVM, Nijmeijer K. Salinity gradients for  
728 sustainable energy: Primer, progress, and prospects. *Environ Sci Technol*  
729 2016;50:12072–94. <https://doi.org/10.1021/acs.est.6b03448>.
- 730 [37] Simões C, Pintossi D, Saakes M, Brilman W. Optimizing multistage reverse  
731 electrodialysis for enhanced energy recovery from river water and seawater:  
732 Experimental and modeling investigation. *Adv Appl Energy* 2021;2:100023.  
733 <https://doi.org/10.1016/J.ADAPEN.2021.100023>.
- 734 [38] Hu J, Xu S, Wu X, Wu D, Jin D, Wang P, et al. Multi-stage reverse electrodialysis:  
735 Strategies to harvest salinity gradient energy. *Energy Convers Manag*  
736 2019;183:803–15. <https://doi.org/10.1016/J.ENCONMAN.2018.11.032>.
- 737 [39] Hu J, Xu S, Wu X, Wang S, Zhang X, Yang S, et al. Experimental investigation  
738 on the performance of series control multi-stage reverse electrodialysis. *Energy*  
739 *Convers Manag* 2020;204:112284.  
740 <https://doi.org/10.1016/J.ENCONMAN.2019.112284>.
- 741 [40] Veerman J. Reverse electrodialysis: Co-and counterflow optimization of  
742 multistage configurations for maximum energy efficiency. *Membranes (Basel)*  
743 2020;10:1–13. <https://doi.org/10.3390/membranes10090206>.
- 744 [41] Veerman J, Saakes M, Metz SJ, Harmsen GJ. Reverse electrodialysis: A validated  
745 process model for design and optimization. *Chem Eng J* 2011;166:256–68.  
746 <https://doi.org/10.1016/j.cej.2010.10.071>.
- 747 [42] Vermaas DA, Veerman J, Yip NY, Elimelech M, Saakes M, Nijmeijer K. High  
748 efficiency in energy generation from salinity gradients with reverse electrodialysis.  
749 *ACS Sustain Chem Eng* 2013;1:1295–302. <https://doi.org/10.1021/sc400150w>.
- 750 [43] Simões C, Pintossi D, Saakes M, Borneman Z, Brilman W, Nijmeijer K. Electrode  
751 segmentation in reverse electrodialysis: Improved power and energy efficiency.  
752 *Desalination* 2020;492:114604. <https://doi.org/10.1016/j.desal.2020.114604>.
- 753 [44] Pintossi D, Simões C, Saakes M, Borneman Z, Nijmeijer K. Predicting reverse  
754 electrodialysis performance in the presence of divalent ions for renewable energy  
755 generation. *Energy Convers Manag* 2021;243:114369.

- 756 <https://doi.org/10.1016/J.ENCONMAN.2021.114369>.
- 757 [45] Simões C, Vital B, Sleutels T, Saakes M, Brilman W. Scaled-up multistage reverse  
758 electro dialysis pilot study with natural waters. *Chem Eng J* 2022;450:138412.  
759 <https://doi.org/10.1016/J.CEJ.2022.138412>.
- 760 [46] Doornbusch GJ, Bel M, Tedesco M, Post JW, Borneman Z, Nijmeijer K. Effect of  
761 membrane area and membrane properties in multistage electro dialysis on seawater  
762 desalination performance. *J Memb Sci* 2020;611:118303.  
763 <https://doi.org/10.1016/j.memsci.2020.118303>.
- 764 [47] Veerman J, Saakes M, Metz SJ, Harmsen GJ. Reverse electro dialysis: Performance  
765 of a stack with 50 cells on the mixing of sea and river water. *J Memb Sci*  
766 2009;327:136–44. <https://doi.org/10.1016/j.memsci.2008.11.015>.
- 767 [48] Tedesco M, Mazzola P, Tamburini A, Micale G, Bogle IDL, Papapetrou M, et al.  
768 Analysis and simulation of scale-up potentials in reverse electro dialysis. *Desalin*  
769 *Water Treat* 2015;55:3391–403. <https://doi.org/10.1080/19443994.2014.947781>.
- 770 [49] Grossmann IE, Caballero JA, Yeomans H. Mathematical programming approaches  
771 to the synthesis of chemical process systems. *Korean J Chem Eng* 1999 164  
772 1999;16:407–26. <https://doi.org/10.1007/BF02698263>.
- 773 [50] Grossmann IE, Trespalacios F. Systematic modeling of discrete-continuous  
774 optimization models through generalized disjunctive programming. *AIChE J*  
775 2013;59:3276–95. <https://doi.org/10.1002/aic.14088>.
- 776 [51] Tristán C, Fallanza M, Ibáñez R, Ortiz I, Grossmann IE. A generalized disjunctive  
777 programming model for the optimal design of reverse electro dialysis process for  
778 salinity gradient-based power generation. *Comput Chem Eng* 2023:108196.  
779 <https://doi.org/https://doi.org/10.1016/j.compchemeng.2023.108196>.
- 780 [52] Tristán C, Fallanza M, Ibáñez R, Ortiz I. Recovery of salinity gradient energy in  
781 desalination plants by reverse electro dialysis. *Desalination* 2020;496:114699.  
782 <https://doi.org/10.1016/j.desal.2020.114699>.
- 783 [53] Ortiz-Imedio R, Gomez-Coma L, Fallanza M, Ortiz A, Ibáñez R, Ortiz I.  
784 Comparative performance of Salinity Gradient Power-Reverse Electro dialysis  
785 under different operating conditions. *Desalination* 2019;457:8–21.  
786 <https://doi.org/10.1016/J.DESAL.2019.01.005>.
- 787 [54] Chen Q, Grossmann IE. Recent Developments and Challenges in Optimization-  
788 Based Process Synthesis. <https://doi.org/10.1146/Annurev-Chembioeng-080615-033546>  
789 2017;8:249–83. <https://doi.org/10.1146/ANNUREV-CHEMBIOENG-080615-033546>.  
790
- 791 [55] EUROSTAT. Electricity prices for non-household consumers - bi-annual data  
792 (from 2007 onwards) [NRG\_PC\_205] n.d.  
793 <https://ec.europa.eu/eurostat/databrowser/bookmark/65f83096-1534-4ddc-a561-44764c07601c?lang=en> (accessed April 3, 2023).  
794
- 795 [56] ICAP. Emissions Trading Worldwide: Status Report 2018. Berlin: 2018.
- 796 [57] ICAP. Emissions Trading Worldwide: Status Report 2019. Berlin: 2019.

- 797 [58] ICAP. Emissions Trading Worldwide: Status Report 2021. Berlin: 2021.
- 798 [59] ICAP. Emissions Trading Worldwide: Status Report 2022. Berlin: 2022.
- 799 [60] ICAP. Emissions Trading Worldwide: Status Report 2023. Berlin: 2023.
- 800 [61] Hart WE, Laird CD, Watson J-P, Woodruff DL, Hackebeil GA, Nicholson BL, et  
801 al. *Pyomo — Optimization Modeling in Python*. vol. 67. Second Edi. Cham:  
802 Springer International Publishing; 2017. [https://doi.org/10.1007/978-3-319-](https://doi.org/10.1007/978-3-319-58821-6)  
803 [58821-6](https://doi.org/10.1007/978-3-319-58821-6).
- 804 [62] Chen Q, Johnson ES, Bernal DE, Valentin R, Kale S, Bates J, et al. *Pyomo.GDP:*  
805 *an ecosystem for logic based modeling and optimization development*. *Optim Eng*  
806 *2021*;1–36. <https://doi.org/10.1007/s11081-021-09601-7>.
- 807 [63] Lee S, Grossmann IE. A global optimization algorithm for nonconvex generalized  
808 disjunctive programming and applications to process systems. *Comput Chem Eng*  
809 *2001*;25:1675–97. [https://doi.org/10.1016/S0098-1354\(01\)00732-3](https://doi.org/10.1016/S0098-1354(01)00732-3).
- 810 [64] Chen Q, Johnson ES, Sirola JD, Grossmann IE. *Pyomo.GDP: Disjunctive Models*  
811 *in Python*. *Comput. Aided Chem. Eng.*, vol. 44, Elsevier B.V.; 2018, p. 889–94.  
812 <https://doi.org/10.1016/B978-0-444-64241-7.50143-9>.
- 813 [65] Forgacs C. Recent developments in the utilization of salinity power. *Desalination*  
814 *1982*;40:191–5. [https://doi.org/10.1016/S0011-9164\(00\)88683-X](https://doi.org/10.1016/S0011-9164(00)88683-X).
- 815 [66] Meyer-Steele S, von Gottberg A, Talavera JL. New Sea Water Reverse Osmosis  
816 Plant for the Carribean “Energy Recovery, Brine Recovery & Cost Reduction.”  
817 2001.
- 818 [67] Portillo E, de la Rosa MR, Louzara G, Quesada J, Ruiz JM, Mendoza H. Dispersion  
819 of desalination plant brine discharge under varied hydrodynamic conditions in the  
820 south of Gran Canaria. *Desalin Water Treat* *2014*;52:164–77.  
821 <https://doi.org/10.1080/19443994.2013.795349>.
- 822 [68] Sadhwani Alonso JJ, Melián-Martel N. Environmental Regulations—Inland and  
823 Coastal Desalination Case Studies. In: Gude VG, editor. *Sustain. Desalin. Handb.*  
824 *Plant Sel. Des. Implement.*, Butterworth-Heinemann; 2018, p. 403–35.  
825 <https://doi.org/10.1016/B978-0-12-809240-8.00010-1>.
- 826 [69] Pérez Talavera J, Quesada Ruiz J. Identification of the mixing processes in brine  
827 discharges carried out in Barranco del Toro Beach, south of Gran Canaria (Canary  
828 Islands). *Desalination* *2001*;139:277–86. [https://doi.org/10.1016/S0011-](https://doi.org/10.1016/S0011-9164(01)00320-4)  
829 [9164\(01\)00320-4](https://doi.org/10.1016/S0011-9164(01)00320-4).
- 830 [70] ICAP. Allowance Price Explorer 2022. <https://icapcarbonaction.com/en/ets-prices>  
831 (accessed May 8, 2023).
- 832 [71] OECD. *Effective Carbon Rates 2021: Pricing Carbon Emissions through Taxes*  
833 *and Emissions Trading*. Paris: OECD; 2021. <https://doi.org/10.1787/0e8e24f5-en>.
- 834 [72] Small Business Innovation Research (SBIR) and Small Business Technology  
835 Transfer (STTR) programs. *Low-Cost Manufacturing of High-Performance Ion*  
836 *Exchange Membranes for Electrodialysis using Initiated Chemical Vapor*

- 837 Deposition n.d. <https://www.sbir.gov/node/2282063> (accessed December 8, 2022).
- 838 [73] IRENA. Renewable Power Generation Costs in 2021. Abu Dhabi: 2021.
- 839 [74] Turek M, Bandura B. Renewable energy by reverse electrodialysis. *Desalination* 2007;205:67–74. <https://doi.org/10.1016/J.DESAL.2006.04.041>.
- 840
- 841 [75] Turek M, Bandura B, Dydo P. Power production from coal-mine brine utilizing  
842 reversed electrodialysis. *Desalination* 2008;221:462–6.  
843 <https://doi.org/10.1016/J.DESAL.2007.01.106>.
- 844 [76] Weiner AM, McGovern RK, Lienhard V JH. A new reverse electrodialysis design  
845 strategy which significantly reduces the levelized cost of electricity. *J Memb Sci*  
846 2015;493:605–14. <https://doi.org/10.1016/j.memsci.2015.05.058>.
- 847 [77] Bevacqua M, Tamburini A, Papapetrou M, Cipollina A, Micale G, Piacentino A.  
848 Reverse electrodialysis with NH<sub>4</sub>HCO<sub>3</sub>-water systems for heat-to-power  
849 conversion. *Energy* 2017;137:1293–307.  
850 <https://doi.org/10.1016/J.ENERGY.2017.07.012>.
- 851 [78] Micari M, Cipollina A, Giacalone F, Kosmadakis G, Papapetrou M, Zaragoza G,  
852 et al. Towards the first proof of the concept of a Reverse ElectroDialysis -  
853 Membrane Distillation Heat Engine. *Desalination* 2019;453:77–88.  
854 <https://doi.org/10.1016/j.desal.2018.11.022>.
- 855 [79] Ranade A, Singh K, Tamburini A, Micale G, Vermaas DA. Feasibility of  
856 Producing Electricity, Hydrogen, and Chlorine via Reverse Electrodialysis.  
857 *Environ Sci Technol* 2022;2022:16062–72.  
858 [https://doi.org/10.1021/ACS.EST.2C03407/ASSET/IMAGES/LARGE/ES2C03407\\_0007.JPEG](https://doi.org/10.1021/ACS.EST.2C03407/ASSET/IMAGES/LARGE/ES2C03407_0007.JPEG).
- 859

860